Development of the AIRIS-WAD Multispectral Sensor for Airborne Standoff Chemical Agent and Toxic Industrial Chemical Detection

William J. Marinelli
Christopher M. Gittins
Bogdan C. Cosofret
Teoman E. Ustun
James O. Jensen

Report Documentation Page

Public reporting burden for the collection of information is estimated to average 1 hour per response, including the time for reviewing instructions, searching existing data sources, gathering and maintaining the data needed, and completing and reviewing the collection of information. Send comments regarding this burden estimate or any other aspect of this collection of information, including suggestions for reducing this burden, to Washington Headquarters Services, Directorate for Information Operations and Reports, 1215 Jefferson Davis Highway, Suite 1204, Arlington VA 22202-4302. Respondents should be aware that notwithstanding any other provision of law, no person shall be subject to a penalty for failing to comply with a collection of information if it does not display a currently valid OMB control number.

1. REPORT DATE **2005**	2. REPORT TYPE	3. DATES COVERED **00-00-2005 to 00-00-2005**

4. TITLE AND SUBTITLE	5a. CONTRACT NUMBER
Development of the AIRIS-WAD Multispectral Sennsor for Airborne Standoff Chemical Agent and Toxic Industrial Chemical Detection	5b. GRANT NUMBER
	5c. PROGRAM ELEMENT NUMBER
6. AUTHOR(S)	5d. PROJECT NUMBER
	5e. TASK NUMBER
	5f. WORK UNIT NUMBER

7. PERFORMING ORGANIZATION NAME(S) AND ADDRESS(ES) **Physical Sciences Inc,20 New England Business Center,Andover,MA,01810**	8. PERFORMING ORGANIZATION REPORT NUMBER

9. SPONSORING/MONITORING AGENCY NAME(S) AND ADDRESS(ES)	10. SPONSOR/MONITOR'S ACRONYM(S)
	11. SPONSOR/MONITOR'S REPORT NUMBER(S)

12. DISTRIBUTION/AVAILABILITY STATEMENT
Approved for public release; distribution unlimited

13. SUPPLEMENTARY NOTES
The original document contains color images.

14. ABSTRACT
see report

15. SUBJECT TERMS

16. SECURITY CLASSIFICATION OF:			17. LIMITATION OF ABSTRACT	18. NUMBER OF PAGES	19a. NAME OF RESPONSIBLE PERSON
a. REPORT **unclassified**	b. ABSTRACT **unclassified**	c. THIS PAGE **unclassified**		**16**	

Development of the AIRIS-WAD Multispectral Sensor For Airborne Standoff Chemical Agent And Toxic Industrial Chemical Detection

William J. Marinelli, Christopher M. Gittins, Bogdan R. Cosofret, and Teoman E. Ustun

Physical Sciences Inc, 20 New England Business Center, Andover, MA 01810,
Voice: 978.689.0003, E-mail: marinelli@psicorp.com

and

James O. Jensen

U.S. Army Edgewood Chemical and Biological Center, ATTN: AMSSB-RRT-DP / E5554
5183 Blackhawk Road, Aberdeen Proving Ground, MD 21010-5424

Abstract

The AIRIS Wide Area Detection System breadboard was employed in an airborne configuration to detect chemical agent stimulant releases during the Technology Readiness Evaluations conducted at Dugway Proving Grounds in July 2002 (TRE-02) and at the Joint Urban 2003 tests at Oklahoma City, OK in July 2003. The observations were conducted from a gyro-stabilized pointing system mounted on a UH-1 helicopter and conducted at ranges up to ~ 7 km and altitudes to 1000 feet in conjunction with the Redstone Technical Test Center. Additional test data will be reported from ground measurements conducted during the TRE-02 and the Pentagon Shield test. In all cases the sensor a comprised 64 x 64 element HgCdTe detector array coupled to AIRIS tunable filter resulting in a system with nominal 10 cm^{-1} spectral resolution and a 0.8 milliradian IFOV. The measured NESR for the system ranged from 2 to 3 μW/(cm^2 sr μm). Observations were made of the chemical stimulant SF$_6$ and the biological simulant BG. In this paper we will report on quantitative observations of these releases as well as the conversion of the breadboard sensor to a field prototype. The analysis will focus on the ability to detect the releases using various algorithms and tracking of the releases through urban environments.

1.   Introduction

The development of the AIRIS Wide Area Detector prototype was preceded by a series of ground and airborne tests using several generations of breadboard systems. The goals of these tests ranged from determining the feasibility of the basic concept, to the demonstrating the ability to deploy in rotorcraft, to the evaluation of the passive infrared remote sensor approach for the detection of biological aerosols and liquid chemical agents on surfaces. The history of field testing of the AIRIS technology and key results of those tests is provided in Table 1.

In this paper we provide an overview of the results of three of the most recent of these tests followed by a description of the prototype sensor. The Technology Readiness Evaluations 2002 (TRE-02) experiments involved imaging a series controlled chemical vapor and biological aerosol releases at the US Army Dugway Proving Grounds. Releases were viewed from an AIRIS system contained in a pod, known as "Fat Boy," mounted on a UH-1 helicopter. Observations of releases we made at ranges as great as 5 km on tracks moving both upwind and downwind with respect to the release point. The Joint

Urban 2003 tests were conducted to test the ability to detect chemical releases in urban environments. A modified version of the same sensor platform used in the TRE-02 tests was deployed to Oklahoma City, OK in July 2003 to view SF_6 releases for this test at ranges to about 1 km. Finally, Pentagon Shield was a ground based test designed to measure atmospheric dispersion from a possible chemical or biological release near the Pentagon. A ground based variant of the AIRIS sensor was deployed to determine its ability to remotely detect and track the initial release. Following a description of the technology, the results of each of these tests will be discussed.

Table 1. Summary of AIRIS Field Test History

Test	Year	AIRIS Sensors Deployed	Major Accomplishments
Nighthawk	1999	Ground-based 64 x 64 pixel system	Field test proof of concept against CWA simulants.
Owl	2000	Ground-based 64 x 64 pixel system	Validated system improvements.
Pronghorn	2001	Ground based 64 x 64 and 256 x 256 pixel systems	1) Demonstrated simultaneous multiple CWA simulant detection. 2) Demonstrated passive ranging to release. 3) Showed high P_D and low P_{FA} for reduced number of wavelengths used in detection. 4) Demonstrated direct chemical imaging of DMMP release.
Technology Readiness Evaluations	July 2002	Airborne (UH-1) and ground based 64 x 64 pixel systems	1) Detected release of SF_6 from UH-1. 2) Detected release of BG from ground at 3 km.
AG46 Liquid Agent Detection Trials	September 2002	Ground-based 64 x 64 pixel system	Detected VX, HD, and non-traditional agents on selected surfaces.
Joint Urban 2003	July 2003	Airborne (UH-1) 64 x 64 pixel system	Detected release of SF_6 simulant released in downtown Oklahoma City.
Preliminary Hemisphere Trials	March 2004	Two ground based 64 x 64 pixel systems	1) Detected SF_6 to 350 meters down wind of release. 2) Demonstrated computed tomography for plume concentration determination.
Pentagon Shield	May 2004	Ground-based 64 x 64 pixel system	Detected release of SF_6 from I-395 simulating attack on Pentagon.

2.   Technology Overview

Passive sensing of CB stimulant releases requires exploitation of both the spectral signatures of the target species as well as the radiance contrast between the release plume and the background scene. The AIRIS sensors are comprised of an LWIR focal plane array-based camera which views the far field through a low-order, tunable Fabry-Perot etalon.[1,2] The tunable etalon provides the spectral resolution necessary to resolve structured absorption and emission from molecular vapors and aerosols. The focal plane array (FPA) enables radiance measurements of sufficient accuracy that chemical vapors and aerosols may be selectively detected with only several degrees effective temperature difference between the vapor and the background.

We analyze the multispectral imaging data using algorithms developed at PSI. Previously, we have shown two key sensor capabilities:

- Selective detection of one and two chemical species in plumes containing multiple species
- Detection of a single species with low false alarm rate using a limited number of detection bands.

In this paper we will highlight our observations of SF_6 and BG aerosol clouds against terrestrial and low sky backgrounds.

A schematic illustration of the complete AIRIS optical train is depicted in Figure 1. The sensor design was developed by PSI and is described in prior publications.[1-7]
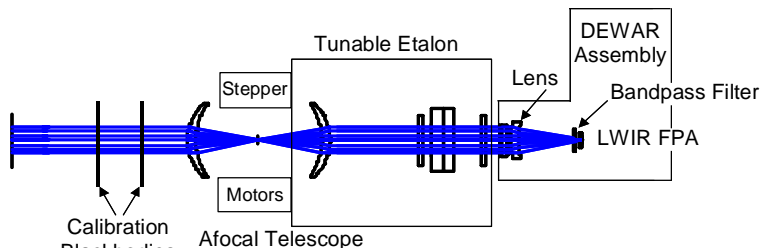

Figure 1. Schematic illustration of AIRIS optical train.

The Fabry-Perot interferometer (etalon) enables the sensors' hyperspectral capabilities. It operates as a tunable interference filter which selects the wavelength that illuminates the FPA. This configuration affords both wide field-of-view and broad spectral coverage. A bandpass filter is placed in front of the FPA to limit its response to a single etalon transmission order. Figure 2 depicts measured etalon transmission and spectral resolution (FWHM) over the etalon's operating range. There are ~40 spectral resolution elements over the interferometer's operating range. Although the second order (m=2) fringe may be continuously scanned to provide coverage of the 8 to 11 μm region, we have found that combined operation in m=3 (8 to ~10 μm) and m=2 (~10 to 11 μm) provides a better trade-off between spectral resolution and optical throughput for the chemical imaging applications investigated to date. The spacing and alignment of the etalon mirrors is controlled via a closed-loop control system. The etalon can be tuned between resolution elements in 20 to 30 ms while maintaining wavelength positioning accuracy of ~1 cm^{-1}. The AIRIS system control program is derived from the software used to control the instrument's LWIR camera. Etalon control is accomplished within the system control program. Each AIRIS system computer is an Intel Pentium-based PC with Windows NT 4.0 as the operating system.
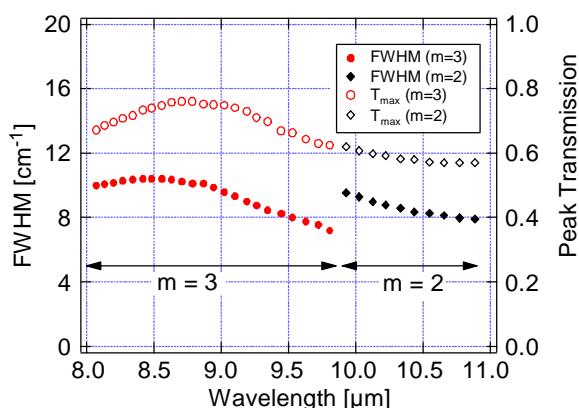

Figure 2. Peak etalon fringe transmission and FWHM as a function of wavelength; m = 3 fringe from 8.0 to 9.8 μm and m = 2 fringe from 9.9 to 10.9 μm.

Two variants of the sensor have been developed. The properties of the two sensor variants are identical except for their LWIR cameras. One sensor utilizes a 64 x 64 element HgCdTe FPA-based camera (Santa Barbara Focalplane, Goleta CA) and the second implements a 256 x 256 element HgCdTe FPA-based camera (Santa Barbara Focalplane, Goleta CA). Table 2 lists the salient characteristics of each instrument's camera and optical train.

The 50 mm Ge lens located in front of the FPA results in an f/2.4 optical train. The lens provides diffraction limited focal spot size (~1 pixel) on-axis and ~2 pixels blurring (astigmatism) at the corners of the 64 x 64 pixel FPA. The imaging quality is high over the central ~200 x 200 pixels of the larger FPA, however the

Table 2. AIRIS-CW Characteristics

Property \ Instrument	64 x 64 FPA-based	256 x 256 FPA-based
Pixel pitch [μm]	61	40
Afocal telescope magnification	3:2	3:2
IFOV [mrad]	0.80	0.53
Field-of-regard [deg x deg]	3.0 x 3.0	7.8 x 7.8
FPA readout	rolling	snapshot
Camera frame rate [Hz]	21.3	114.9
FPA integration time [ms (typ.)]	1.44	0.56
A/D dynamic range [bits]	14	14

r.m.s. blur spot diameter is ~7 pixels at its corners.   The 3:2 afocal telescope located beyond the tunable etalon module provides a fine adjustment of the system focus. Two calibration blackbodies are mounted on a rotation stage and enable collection of radiometric calibration data. The high temperature blackbody is normally operated 10 to 15 K above ambient temperature and the low temperature blackbody operated ~5 K below ambient. The blackbodies are used to generate two point radiometric calibrations (gain and offset) for each pixel at each wavelength viewed. The calibration blackbodies are rotated clear of the system field-of-view during normal operation.

The entire optical train is mounted on a servo-controlled optical bench in the Fat Boy pod that is slaved to a pointing and tracking system that allows the operator to lock on to a specific point on the ground and obtain multispectral data over the system field of view. Figure 3 shows a detailed view of the sensor in the Fat Boy.

Electronics to operate the system were mounted in a rack system located in the passenger/ cargo compartment of a UH-1 helicopter with cables running through the rack to the pod through a bundle strapped to the aircraft exterior. A photograph of the rack system for control of the sensor is shown in Figure 4. Power for the system was provided by a 28VDC to 120VAC inverter (ProSine) and coupled to the AIRIS system via an uninterruptible power supply (American Power Conversion).

Figure 3. Photograph of Fat Boy with aerodynamic skins off showing AIRIS-LW (upper right, Turbo-FT (upper left), IR camera for tracking (lower left) and intensified visible camera for tracking (lower right).

Figure 4. Photograph of UH-1 cabin with AIRIS equipment mounted to the left. Shown from top to bottom are the monitor, keyboard, computer, power supply, and UPS.

3.   Technology Readiness Experiments 2002

Two series of releases were observed at the TRE-02 tests. All releases viewed in these measurements were conducted at fixed locations along Highway 101 with respect to the ground observation site at the intersection of Highway 101 with Victory Road. Biological aerosols were detected from ground observations conducted from the command post site at the intersection of Highway 101 with Victory Road. Airborne data acquisition during the TRE experiments was accomplished, for the most part with this system, by locking the Fat Boy tracking system on to a fixed location on the ground at or downwind of the release point and then acquiring spectral data cubes during the releases as the UH-1 slowly (typically 10-20 kt) traversed either upwind or downwind with respect to the release point. The wind direction during these releases was generally south to north moving along Highway 101 towards the ground observation point. The Fat Boy was limited to look down angles of 22.5 degrees from horizontal. The typical flight altitude was 300 meters, resulting in a minimum standoff distance of approximately 750 meters. The terrain at the site is one of desert floor, sparsely covered by scrub brush with a height of approximately 2 feet.

Releases occurred over periods as long as 5 minutes. Prior to each release the system was calibrated radiometrically using the two on-board blackbody calibrators. Subsequent to the calibration data was acquired during both up wind and down wind legs commencing with initial lock on to the release point and ending with loss of lock at a point where the look down angle exceeded 22.5 degrees. During this period the helicopter traveled approximately 4 km. After loss of lock the system was again calibrated radiometrically with the blackbodies. As many as 8 data cubes were acquired during a typical data collection pass. However, on several of the data cubes the tracking system would jitter and loose lock during acquisition events due to the low contrast in the scene, leading to a shift in the location of the target in the image with each wavelength image in the data cube.

Chemical Simulant Releases

The hyperspectral data cubes generated using AIRIS consisted of 36 narrowband images: 1260 cm^{-1} (7.94 µm) to 910 cm^{-1} (10.99 µm) in 10 cm^{-1} increments with the 64 x 64 system. The initial analysis was conducted by applying the absolute radiometric calibration to the data and then analyzing regions of interest for spectral content. The initial algorithm allowed the user to define a region of the scene representative of the local background and then subtracted the background spectrum from each pixel in the data cube to obtain a net change in radiance from the background. This differential radiance data cube was then analyzed for spectral content by looking for matches with the SF_6 spectrum using a spectrally matched filter approach. Sample data from the data cube 20726c8 is used to illustrate the approach. This data cube was acquired during a release of SF_6 that occurred continuously for 5 minutes with a total release of 38 kg or a release rate of 127 grams/second. Wind speed during the release was 1.4 meters/second and turbulence was low.

Figure 5. Radiance image of SF_6 release at 10.6 µm showing roads and SF_6 plume moving diagonally across the upper right corner of the image.

An image of the scene recorded at 10.6 um, at the peak of the SF_6 absorption band, is shown in Figure 5. The data shows a rather monotonic background interrupted by roads seen moving through the scene from bottom center to top right. Note that the roads are darker, and hence apparently cooler that the rest of the scene, which is dominated by the
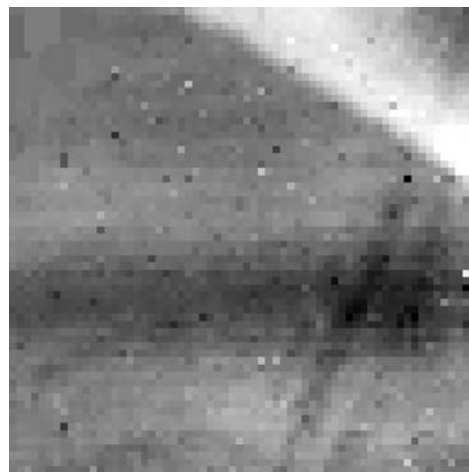
5

vegetation. While some of this apparent temperature differential may be due to emissivity differences between the two surfaces, it is also true that vegetation more closely reaches the air temperature due to the motion of the wind through the leaves. The upper right corner of the image shows a white streak moving through the scene which can be identified as the plume from the SF_6 release. The region in the top left of the image, outside of the plume area, was used to obtain the background. The spectral data from that region was fit to the Planck blackbody function, assuming unit emissivity, and found to have a radiance temperature of approximately 285 K (11.8 degrees C). Air temperature that evening was measured to be 25 degrees C; hence an apparent ΔT of approximately 13 degrees existed between the background and the air.

The subtraction of the background radiance from the entire data cube results in the cancellation of much of the background radiance but not the differential signal from the road underlying the SF_6 release plume. The spectrum of the background subtracted region indicates that the accuracy of the subtraction is on the order of ~10 µW/(cm^2 sr^{-1} µm^{-1}). For the case of a single chemical species in an optically thin plume, the differential radiance at the sensor with and without the plume present is:

$$\Delta N(\lambda)_{sens} = N_{plume}(\lambda) - N_{bkgd}(\lambda) \approx \sigma(\lambda) \cdot \rho L \cdot \left[\frac{dN}{dT}\right]_{T_{bkgd}} \cdot \Delta T \qquad (1)$$

where σ is the chemical's absorption coefficient, ρL is its column density, the quantity in brackets is the derivative of the Planck function with respect to temperature (~16 µW/(cm^2 sr µm K) at 10 µm and 300 K), and ΔT is the effective temperature differential between the plume and the background. The data in Figure 6 shows a differential radiance of about 70 µW/(cm^2 sr^{-1} µm^{-1}) while the SF_6 absorption coefficient, derived from a resolution degraded HITRAN spectrum of SF_6 is 2.5 x 10^{-3} ppmv^{-1} m^{-1}. Inversion of Equation 1 to obtain an apparent SF_6 column density was done assuming a 13K radiance temperature differential, i.e. it was assumed that the SF_6 was equilibrated with the air temperature. This analysis resulted in an assignment of the SF_6 column density of approximately 140 ppmv-m.
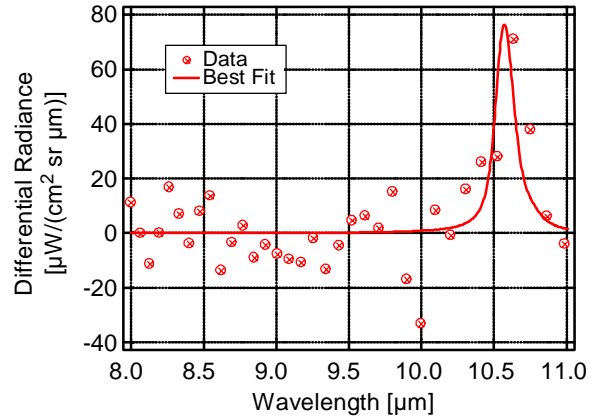

Figure 6. SF_6 spectrum recovered from spectrally matched filter analysis.

Biological Simulant Releases

Both continuous and puff releases of BG were captured during the 25 July 2002 data collection events. Figure 7 shows annotated thermal infrared imagery from a BG puff release measured at a range of 3 km while Figure 8 shows the spectrum in the regions identified as the background and cloud in Figure 8. We have previously reported on an effort to model the signature of the aerosol cloud[8] and developed an approach that explains the signature in terms of increased scattering of colder thermal radiation from the sky replacing warmer low-sky thermal radiation in regions of the spectrum where the aerosols have a higher scattering efficiency. Figure 9 shows a result of the modeling effort to replicate the observed signature.
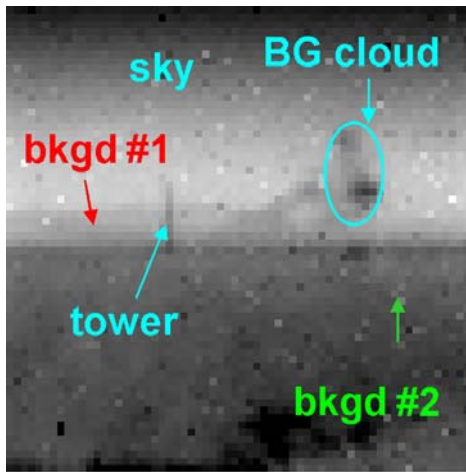
Figure 7. Infrared image of BG puff release showing cloud and regions used as background in spectral analysis.

Figure 8. Differential spectrum of each of the regions identified in Figure 8 showing apparent signature of BG cloud.
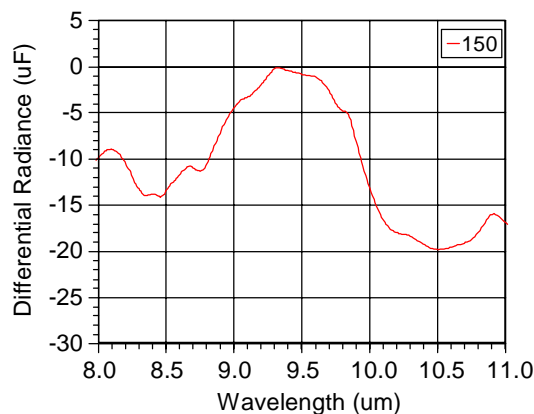

Figure 9. Model prediction of BG cloud signature based on calculated scattering properties of BG spores and radiative transfer model including scattering.

4.   Joint Urban 2003

Releases of the simulant SF_6 were conducted at a rate of 3 grams per second from a major intersection in downtown Oklahoma City. Figure 10 shows a photograph of the release point from an altitude of 2000 ft and approximately 1 km downwind. Wind in the area of the release was from the south (top of Figure 10) and highly turbulent. A GPS-based tracking system was used with the Fat Boy pod; however, the performance of the tracker was problematic and much of the tracking was done by hand, leading to a significant amount of jitter in some of the acquisitions. This jitter results in a mis-registration of the band-sequentially acquired imagery. Two analysis approaches, spectrally matched filter and two-band correlation, were applied to the imagery. The two-band correlation approach proved to be slightly better at minimizing false alarms in the analysis. Figure 11 shows one of the better detections obtained during the testing. The release vehicle location is indicated by the green circle in the image while the detected plume is indicated by the red shaded areas.

In almost all of the imagery the plume rapidly dissipates upon entry into the street intersection where the release was conducted due to the rapid dilution of the SF_6 in the turbulent flow. Two persistent and interrelated issues were identified in the analysis of this data. The scene radiance dynamic range was high, with emission simultaneously observed from solar heated pavement and cold sky reflected off metal roofs in the same scene. A wide range of material emissivities and sharp discontinuity in transitions to each type of material leads to a high degree of spatial and spectral clutter. Since the detection of chemical releases involves the differentiation of spectral radiance on the order of 1 to 2 percent of the total scene radiance, it is clear that the background radiance at each wavelength must be estimated with a high degree of fidelity. The ability to perform this estimation is compromised when vehicle motion or poor tracking
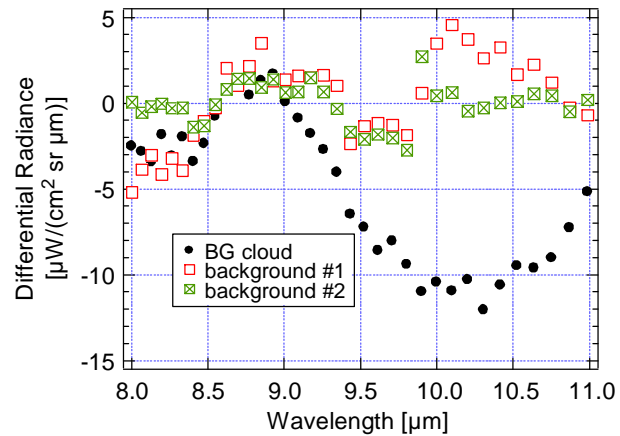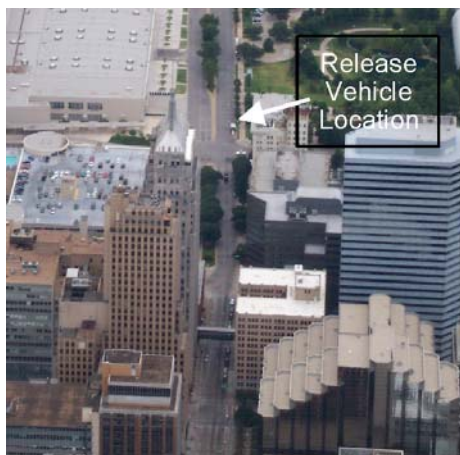
7

Figure 10. Aerial photo of downtown Oklahoma City showing location of release vehicle for Joint Urban 2003.
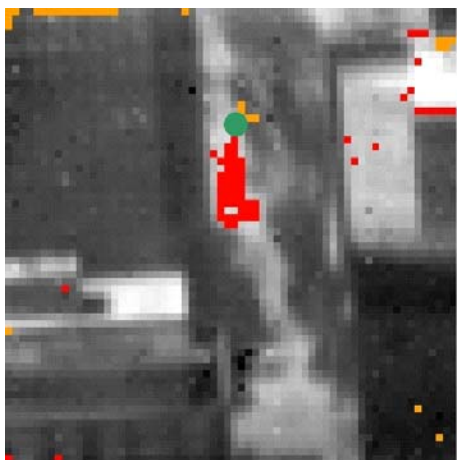

Figure 11. Infrared image from AIRIS data cube with locations of the detection of SF_6 shown in red in the image. The green dot indicates the location of the release vehicle.

performance causes a spatial mis-registration of the imagery as a function of wavelength. These issues were primary contributors to the appearance of false alarms. False alarms were most noted at building edges, on roofs, in windows, and along tree lines. In the development of the AIRIS Wide Area Detector prototype these issues were addressed through improved background estimation algorithms and a data acquisition rate with is 20 times faster than in the breadboard system used to acquire this data.

5. Pentagon Shield

The Pentagon Shield test involved measurements over a single day in which the simulant SF_6 was released from a vehicle moving along I-395 along the south side of the Pentagon. The AIRIS sensor breadboard was positioned in the south parking lot so as to observe the passage of the vehicle. Figure 12 shows and overhead view of the Pentagon indicating the path of the release and the approximate field of view of the sensor. A data cube was acquired every 15 seconds, the cube analyzed, and the results of the detection algorithm presented to the user as a red-flagged detection pixels overlaid on a thermal image of the scene. Figure 13 shows an approximate visual representation of the sensor field of view (left) with major features indicated along with a thermal image showing the detection of a release occurring at 10:15A on 1 May 2004. Releases were conducted every 15 minutes over a 2 hour period in this test entry. The release of the SF_6 simulant was detected in every excursion in which the sensor monitored the highway. However, the sensor data also showed that the dispersion of the simulant was rapid and fell below the sensor detection limit within approximately 45 seconds of release. The data shows a line release observed along the highway. The time series data shows false alarms similar to those found in Oklahoma City, especially along the edges of the road signs on I-395. Since platform motion was not an issue in these measurements, the ability to estimate the background can be identified as the primary cause of the false alarms. We note that, since this is a time series measurement, a future implementation of this technology could make use of the false detection history to improve real-time detection capability.
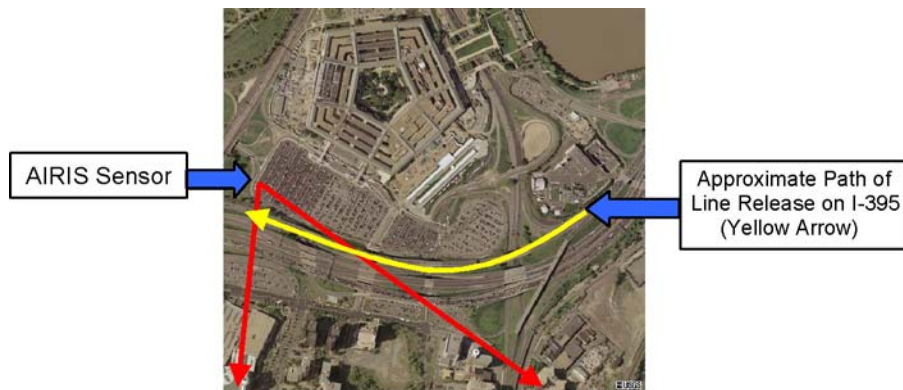
8

Figure 12. Overhead view of the Pentagon
(http://www.terraserver.microsoft.com) with path of
release vehicle and sensor field of view indicated.

Figure 13. Visible photograph providing frame of reference for sensor field of
regard (left) and infrared image with SF_6 release detection indicated from
AIRIS sensor (right).

6. AIRIS-WAD Prototype Development

6.1 Overview

Under funding from the US Army Edgewood Chemical and Biological Center and the Defense Threat Reduction Agency, Physical Sciences Inc (PSI) is developing its Adaptive Infrared Imaging Spectroradiometer technology (AIRIS) as a candidate for the Joint Service Wide Area Detector and related standoff chemical warfare agent (CWA), toxic industrial chemical (TIC), and biological warfare agent aerosol detection, identification, and tracking applications.

The prototype, shown in Figure 14, is a fieldable sensor system having a 32 x 32 degree FOV direct imaging "Camera Mode" and a 360 x 30 degree field of regard (FOR) "Scanning Mode" when equipped with a rotary turntable. The high spatial

Figure 14. Photograph of AIRIS-WAD sensor unit.

9

resolution of the system is achieved by utilizing a 256 x 256 element HgCdTe FPA subtending the 32 x 32 degree FOV to provide a diffraction-limited 2 milliradian IFOV per pixel. The prototype has been designed to meet MIL-810-F for thermal, shock, vibration, and weather and MIL-461/462 for EMI. The system comprises a Sensor Unit (SU), Operator Display Unit (ODU), and Power Unit (PU). The 360 x 30 degree FOR is achieved by positioning the SU FOV in 12 orientations around the compass over a 90 second interval using a rotary turntable. The PU operates using 120VAC line current or 20-32VDC power. The AIRIS-WAD prototype system will have the following capabilities:

- Provide passive detection and tracking of CB releases at ranges to 5 km with 10 meter spatial resolution.
- Provide detection of nerve (VX, GA, GB, GD, GF at 135 mg/m2) and blister (HD, HN3, L at 3,300 mg/m^2) agents in desert, urban and spatially cluttered environments with detection probabilities exceeding 0.9 and false alarm probabilities less than 10^{-4}, both per measurement.
- Incorporate detection of TICs at the level defined as severe in USACHPPMs Toxic Industrial Chemicals Info Card.
- Incorporate detection of compounds associated with the production of CB agents to provide intelligence on production activities and post strike damage assessment.
- Provide RADAR-style plots and direct image display of the environment with JWARN interface.
- Provide real-time acquisition and processing of 32° x 32° CB images at 5 images/second and 360° azimuth x 30° elevation coverage in 90 seconds
- Enable Stryker/Fox vehicle integration and provide a roadmap for UH-1/60, C-130/UAV deployment.
- Design and construct to sensor system prototypes to meet MIL-STD-810F for shock, vibration, drop, immersion, and temperature and MIL-STD-461/462 for EMI.

PSI has developed a draft operational requirements document (ORD) for AIRIS-WAD that closely follows the Commercial JSLSCAD ORD. However, this document includes capabilities inherent in the AIRIS-WAD system and reflects the need for higher spatial resolution and higher data acquisition speeds to perform "on the move" detection. Future field tests of the AIRIS technology will transition to the AIRIS Wide Area Detector prototype. The AIRIS breadboard systems will continue to be used as test beds for the development of new standoff detection approaches and applications.

The sensor unit comprises a 256 x 256 element HgCdTe FPA and its drive electronics, the AIRIS tunable filter and its drive electronics, a 5 element expansion telescope to provide a diffraction limited image over a 32 x 32 degree field of view, an FPGA/DSP based image processor unit, a system controller, and a combined blackbody calibrator/prism actuator. Each of the sub-systems will be described later in this paper. The layout of the sensor components in the system chassis is shown in Figure 15. The total system weight of the optical components and control/data processing electronics is approximately 57 lbs. During steady state operation approximately 150 watts of power is dissipated within the sensor unit, of which about 70 watts is from the detector cryocooler and the remainder from the electronics. The sensor unit is air-cooled and uses a series of heat pipes to pass heat to the rear of the chassis, where a high efficiency heat sink/fan combination is used to maintain all system components within allowed operating temperature limits under environmental temperatures up to 49 degrees C.
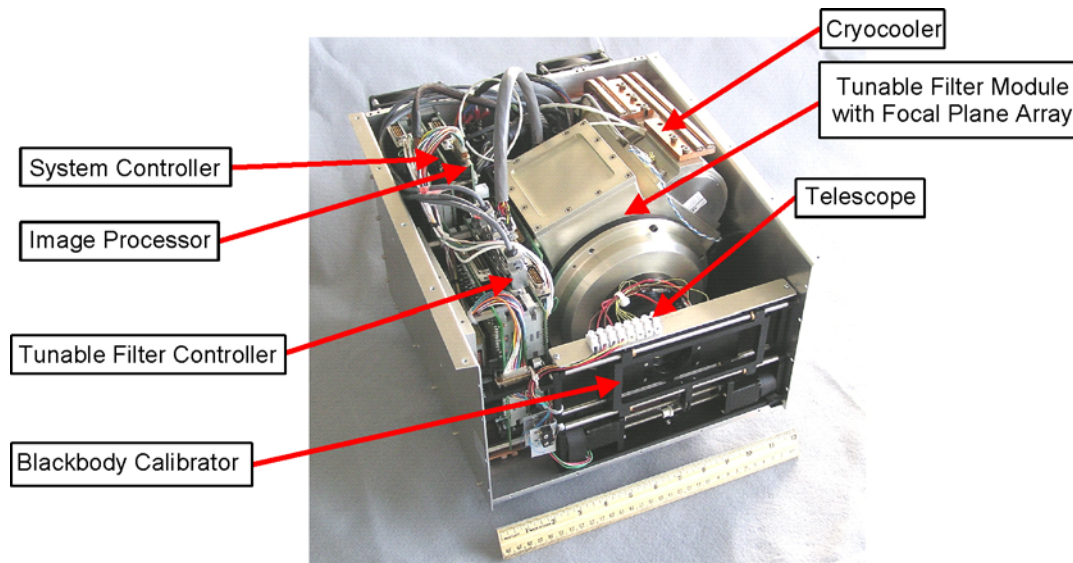
Figure 15. Annotated photograph of system chassis indicating system components and placement.

6.2   Sensor Unit

A photograph of the integrated FPA and tunable filter system is shown in Figure 16. The system's 256 x 256 element HgCdTe FPA was specially developed for the AIRIS-WAD sensor by BAE Systems (Lexington, MA), with custom readout electronics made by Vtech Technologies (Andover, MA). The array has optimized spectral response from 8 to 11.2 µm and sensitivity matched to the spectral throughput properties of the AIRIS tunable filter (nominal 60% peak transmission and 10 cm^{-1} spectral bandwidth). A custom bandpass filter on the detector cold shield limits the infrared radiation reaching the detector to a single order of interference from the interferometer. A specially designed 19 mm focal length f/1.2 lens system, integral to the cold shield, provides a collimated field of view for the detector array looking through the closely-coupled Fabry-Perot tunable filter, which is operated at ambient temperature. An integral Stirling-Cycle cryocooler maintains the FPA, cold shield and filter, as well as the lens assembly, at approximately 65K to reduce overall system noise to about 1 µW/(cm^2 sr^{-1} µm^{-1}).
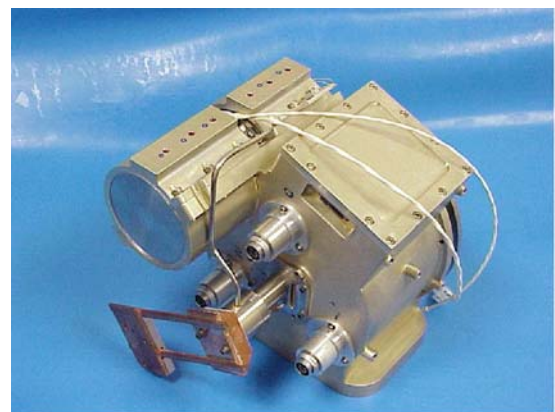

Figure 16. Photograph of sensor module comprising interferometer and focal plane array.

The AIRIS tunable filter module (TFM) utilizes three Burleigh inchworm motors to drive one moving mirror with respect to a fixed mirror. A capacitance micrometry system is used in conjunction with a closed loop control system to position and align the mirrors to transmit a specific wavelength of light to the FPA. Several major improvements have been made to this design over the prior breadboard units. New inchworm drive control electronics have been developed to replace the commercial unit supplied by Burleigh. The new electronics provide the ability to move the actuators on the order of a few microseconds using solid-state power supplies. The mounting arrangement for the mirrors was changed to a flexure system to provide greater lateral stability under high vibration loads as well as greater passive alignment stability. The capacitance micrometry system was improved to provide temperature

11

compensation for improved calibration stability as well as faster readout rates. Finally, the entire control system was moved from a PC-based platform to a dedicated FPGA. The overall impact of these performance improvements was a reduction in wavelength tuning time from 15 ms to approximately 4 ms while achieving a calibration accuracy of 0.5 cm^{-1}. The interferometer is operated in a combination of second and third order to optimize spectral tuning and resolution. Figure 17 shows a photograph of the TFM controller while Figure 18 shows a typical transmission curve for the interferometer.

Figure 17. Photograph of TFM assembly.

Radiometric calibration of the system is provided using an on-board, two temperature blackbody assembly. The assembly comprises two thermoelectrically temperature stabilized blackbody plates located on a precision slider mechanism. The temperatures of the blackbodies are set such that one is approximately 15° C above ambient temperature and the other is approximately 5°C below ambient temperature. Either blackbody can be positioned to fill the field of view of the sensor. At start up, and subsequently periodically during operation, the on-board system controller automatically commands the acquisition of calibration data that is used to apply an individual gain and offset correction for each pixel in the array at each wavelength utilized in the detection algorithm.

Figure 18. TFM transmission spectrum showing nominal 10 cm^{-1} spectral bandwidth and 60% peak transmission.

The algorithm employed in the AIRIS-WAD system is based on the use of Gram-Schmidt ortho-normalized Principal Component basis functions, which are combined with an Orthogonal Sub-space Projection Operator approach to estimate and remove the background spectrum of the scene from the multispectral data. A Spectral Angle mapping approach, in which the correlation between each background-nulled pixel spectrum and the target reference spectrum is determined, is used to test for the presence of a specified target compound. Pixels where both the Spectral Angle correlation and differential radiance relative to the background exceed pre-determined threshold values are identified as corresponding to the target compound. Detection thresholding on the basis of both spectral similarity and intensity reduces the probability of false alarm without significantly degrading the probability of target detection. This algorithm is implemented in a combined FPGA/DSP image processor, jointly developed by PSI and Vtech Technologies, and integrally coupled to the FPA detector to permit high speed detection of the CWAs and their simulants. The processor, shown in Figure 19, comprises a XC2V6000-6BF957C (Virtex II) series FPGA and an ADSP-TS101SAB1-100 DSP (300 MHz TigerSHARC)
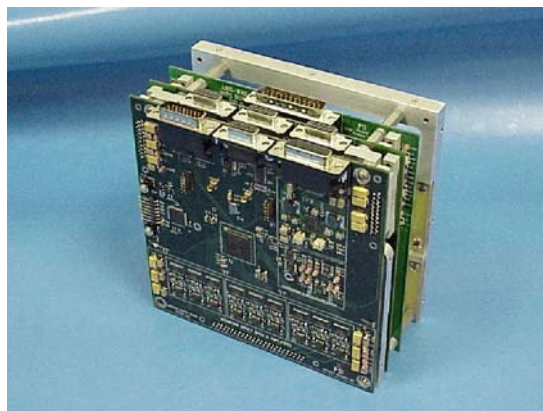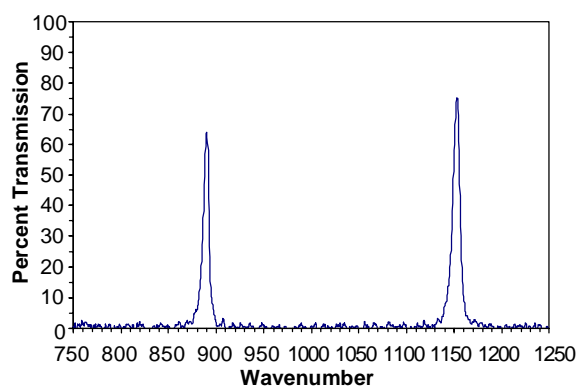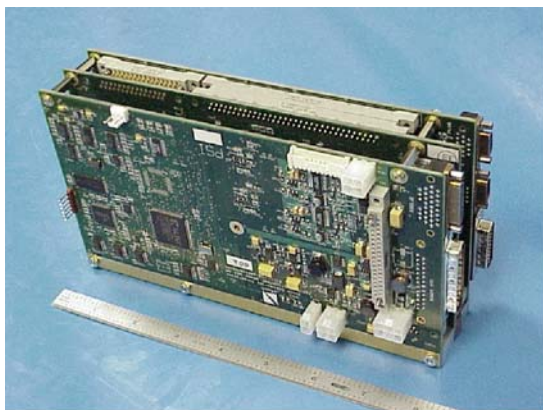

Figure 19. System controller and image processing board assembly.

12

from Analog Devices. The processor can radiometrically calibrate and execute the detection algorithm on a 20 wavelength 256 x 256 pixel data cube at rates exceeding 5 cubes per second. Reduced wavelength data cubes (5 wavelengths) can be processed at near video rates. The DPG/PNNL infrared spectral libraries are used for the detection of CWAs as well as TICs.

6.3   Operator Display Unit

The system ODU is shown in Figure 20. The ODU is based on a MIL-810/461/462-qualified display from L-3 Communications. This unit has dimensions 12" x 10" x 4" and weighs 8 lbs. It can be mounted in a console for various platform integrations or can be used with a mounting stand for stand alone operation. It interfaces to the Sensor Unit through the system controller, which is integral to the Sensor Unit. The ODU uses a menu interface to control system operation through a series of buttons on the front panel. A window on the display shows system status, detection history, any error messages, and communications status. Two display modes are enabled on the ODU: Camera and Scan modes. In the Camera
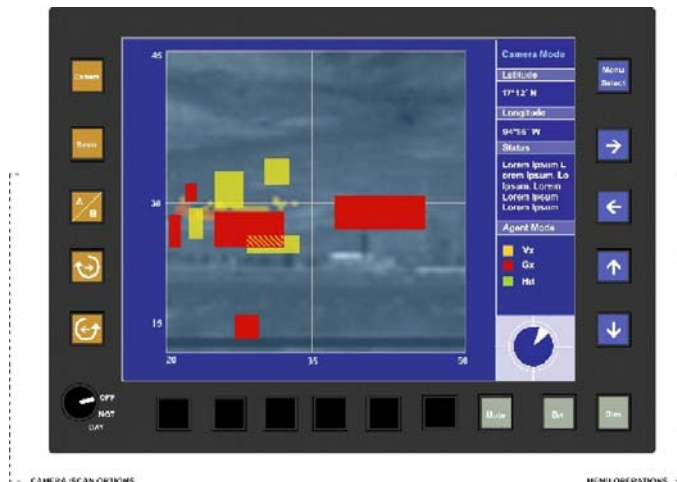

Figure 20. Design for ODU display in Camera Mode as implemented on the L-3 Communications display module.

Mode the field of regard of the sensor is positioned by the platform on which it is mounted or by the on-board rotary table. Individual data cubes are acquired, analyzed for the presence of threat chemicals, and the color coded results of that analysis overlaid on a thermal infrared image of the scene acquired with the sensor.

In Scan Mode the system controller commands a rotary turntable to position the sensor unit to each of 12 positions around a 360 degree circle and acquire data at each position. The results of the analysis of the individual data cubes are stitched together by the system control software and displayed on a RADAR style plot to provide situational awareness. A digital compass on-board the Sensor Unit

provide absolute directional reference and the Sensor Unit is capable of received NMEA 0183 GPS messages to provide absolute positional reference to anchor the RADAR plot display. The RADAR plot can be overlaid on a digital terrain map stored in memory to provide additional situational awareness to the user, as shown in Figure 21.

Additional spatial filtering approaches are used to reduce uncorrelated single pixel and correlated edge-induced false alarms. Images are reduced to a binary format in which detection pixels have a value of unity and non-detection pixels have a value of zero. A two-step dilation and erosion algorithm is first conducted. The dilation operation determines if each pixel has any neighbor that is non zero.
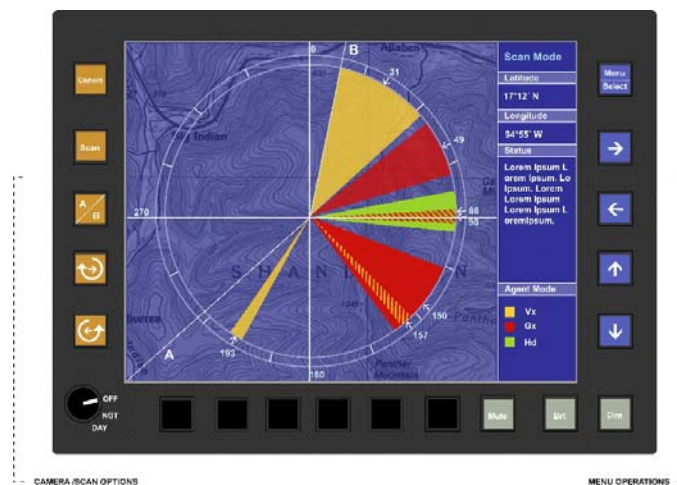

Figure 21. Design for ODU display in Scan Mode as implemented on the L-3 Communications display module.

13

If it has, that pixel also is made non-zero. If not, it remains the same. The dilation operation will fill in gaps in the structure of the chemical cloud due to local turbulence or locally poor thermal contrast, smooth borders, and slightly enlarge the size of the cloud. The erosion process does the opposite of dilation. If any neighbor pixel is zero, the pixel is set to zero. This process reduces the image object to its original size. This sequence will result in smoothed regions of non-zero pixels representing detection clouds. It also suppresses single pixel false alarms. A perimeter function is then applied. The perimeter function keeps all perimeter pixels non-zero, setting all interior pixels to zero. This function defines cloud edges for boundary determination and also suppresses false alarms at edges, where they are typically one pixel wide. Finally, a boundary function is applied that lists the X/Y components of the remaining perimeter pixels. These coordinates are converted into azimuth and elevation boundaries using data from the on-board digital compass and provide the cloud location data for transmission via JWARN and display on the ODU. We note that without the high spatial resolution inherent in the AIRIS-WAD system such operations, and the concurrent reduction in false alarm rate, would not be possible.

7.   Conclusions

The rich history of field testing conducted on the AIRIS breadboard sensor has been responsible for demonstrating the feasibility and clear advantages of a true imaging passive infrared standoff sensor as well as providing guidance for the development of the highly integrated AIRIS Wide Area Detector Prototype. Cumulatively, including tests not discussed in this paper, field testing has demonstrated:

- The ability to detect chemical simulants from both ground and airborne (UH-1) platforms at relevant quantities in relevant environments (desert, urban, and treed areas).
- Data suggesting that biological aerosols can be detected at the time of release and that deployed passive infrared multispectral sensors can play some role in biological defense alone, or more appropriately, as cueing agents for higher sensitivity LIDARs.
- Under certain circumstances passive infrared multispectral imagery can be used to remotely detect liquids, including chemical agents, on surfaces.
- Improvements in detection algorithms, now underway, are required to reduce false alarm rates in cluttered urban environments, but that the high spatial resolution of the AIRIS sensor is required to detect smaller scale (non-battlefield) releases in these environments.
- Multispectral data cube image registration is a critical factor in the detection of small scale releases, especially in urban scenes and that corrections for platform motion are required. In the development of the AIRIS Wide Area Detector we have improved that capability by acquiring data cubes in less than 200 ms. Future enhancements may further reduce that time by a factor of three. We are also exploring software approaches to image registration using the data cube imagery that can be implemented in a FPGA data processor.

The AIRIS-WAD sensor is currently completing its test and integration phase. Key elements of the system have already met their performance goals. Two additional units are currently being produced for evaluation under the DT-JSLSCAD trials to be conducted in 2005. In addition to the DT-JSLSCAD trials in 2005, an AIRIS-WAD sensor prototype will be installed in a GPS-directed POD on a UH-1 helicopter and flown in pseudo-UAV mode in which detection data will be telemetered to a ground station. Additional tests are planned to probe the detection of biological aerosols and toxic industrial chemicals.

9.   References

1.   Gittins, C.M., Lawrence, W.G., and Marinelli, W.J., "Frequency-Agile Bandpass Filter for Direct Detection LIDAR Receivers," *Applied Optics* 37, 8327 (1998).

2.   Marinelli, W.J., Gittins, C.M., Gelb, A.H., and Green, B.D., "A Tunable Fabry-Perot Etalon-Based Long Wavelength Infrared Imaging Spectroradiometer ," *Applied Optics* 38, 2594 (1999).

3.   C.M. Gittins, L.G. Piper, W.T. Rawlins, W.J. Marinelli, James O. Jensen, and Agnes N. Akinyemi, "Passive and Active Standoff Infrared Detection of Bio-aerosols," Field Analytical Chemistry and Technology, May 1999.

4.   Marinelli, W.J., Gittins, C.M., and Jensen, J.O., "Passive Multispectral Imaging for Standoff Chemical Detection," MASINT Chemical Warfare Science and Technology Symposium, San Diego, CA, August 2000.

5.   Gittins, C.M. and Marinelli, W.J., "Remote Characterization of Chemical Vapor Plumes by LWIR Imaging Fabry-Perot Spectrometry," Fifth Joint Conference on Standoff Detection for Chemical and Biological Defense, Williamsburg, VA, 24-28 September 2001.

6.   Marinelli, W.J., Gittins, C.M., and Jensen, J.O., "Sensor Performance Needs for Wide Area Hyperspectral Chemical Agent Detection," Fifth Joint Conference on Standoff Detection for Chemical and Biological Defense, Williamsburg, VA, 24-28 September 2001.

7.   Jensen, J.O., Marinelli, W.J., Gittins, C.M., Ben-David, A., Theriault, J., Bradette, C., and Samuels, A., "Detection of Non-volatile Liquids on Surfaces Using Passive Infrared Spectroradiometers," Fifth Joint Conference on Standoff Detection for Chemical and Biological Defense, Williamsburg, VA, 24-28 September 2001.

8.   Gittins, C.M., Cosofret, B.R., and Ustun, T.E., "Passive Infrared Sensing of Bioaerosol Clouds," SPIE Vol. 5268.